J|A|C|S
ARTICLES

Published on Web 08/17/2010

Catalysis of Transesterification by a Nonfunctionalized Metal−Organic Framework: Acido-Basicity at the External Surface of ZIF-8 Probed by FTIR and *ab Initio* Calculations

Céline Chizallet,*,† Sandrine Lazare,† Delphine Bazer-Bachi,† Fabien Bonnier,† Vincent Lecocq,† Emmanuel Soyer,‡ Anne-Agathe Quoineaud,‡ and Nicolas Bats†

Direction Catalyse et Séparation and Direction Physique et Analyse, IFP Energies Nouvelles, IFP-Lyon, BP3, 69360 Solaize, France

Received April 21, 2010; E-mail: celine.chizallet@ifpenergiesnouvelles.fr

Abstract: The zeolite imidazolate framework ZIF-8 is shown for the first time to be able to catalyze transesterification of vegetable oil with significant activity. Rationalization of this behavior at the atomic scale is provided by combining CO adsorption monitored by FTIR and DFT calculations (clusters and periodic models). We demonstrate that the acido-basic sites are located at the external surface of the material or at defects, but not in the microporosity of ZIF-8. A great variety of sites are found the surface: OH and NH groups, hydrogenocarbonates, low-coordinated Zn atoms, and free N^- moieties belonging to linkers. Their proportions depend on the operating conditions (temperature and pressure). The acido-basicity of the surface is then probed by adsorption of CO at low temperature. In parallel, the species present are mapped by DFT calculations combined with a thermodynamic model. An assignment of the CO region of the FTIR spectra can thus be proposed. The complex infrared spectrum is attributed to the coexistence of classical C-adducts of CO with acid sites and other modes on basic sites (O-adducts and side-on adducts). Adsorption energies and CO frequency shifts show that some strong Lewis sites exist (in particular Zn_{II} species), as well as strong Brønsted acid sites (NH groups), together with basic sites (OH groups and N^- moieties). By calculating the co-adsorption of a model ester (methyl acetate) and methanol, we show the prevailing role of Zn_{II} species as acid sites, combined with N^- moieties and OH groups as basic ones, in determining the catalytic properties of ZIF-8. This work opens new perspectives on the use of MOFs in catalysis and, more generally, on the properties of their external surface.

1. Introduction

Metal−organic frameworks (MOFs) have attracted growing interest in the scientific community since the pioneering work on these solids in the 1990s (see refs 1−12 and references therein for some examples). These materials consist of metallic nodes bonded by organic linkers.[8,9] Multiple combinations between metal cations and various organic linkers make it possible to design an outstanding range of potential structures,[13] having numerous tunable properties. Accordingly, these hybrid crystalline materials have potentially broad applications in fields including sensing,[14] storage and separation of gases,[15−17] optics,[14,18] magnetism,[14,18] and drug delivery.[19] Very recently, motivated by the pioneering work of Fujita and co-workers,[2] this versatility was echoed in the field of catalysis,[10−12] driven by the need for well-defined species that are able to catalyze a variety of single steps, from acido-basic to redox reactions. Promising catalytic activities of MOFs have been reported for reactions catalyzed by organometallic centers,[20−27] and by Brønsted acids[5,28−31] or bases,[32−35] either present or grafted in

† Direction Catalyse et Séparation.
‡ Direction Physique et Analyse.

(1) Gable, R. W.; Hoskins, B. F.; Robson, R. *J. Chem. Soc., Chem. Commun.* **1990**, 1677–1678.
(2) Fujita, M.; Kwon, Y. J.; Washizu, S.; Ogura, K. *J. Am. Chem. Soc.* **1994**, *116*, 1151–1152.
(3) Kepert, C. J.; Rosseinsky, M. J. *Chem. Commun.* **1998**, 31–32.
(4) Eddaoudi, M.; Li, H.; Reineke, T.; Fehr, M.; Kelley, D.; Groy, T. L.; Yaghi, O. M. *Top. Catal.* **1999**, *9*, 105–111.
(5) Evans, O. R.; Ngo, H. L.; Lin, W. *J. Am. Chem. Soc.* **2001**, *123*, 10395–10396.
(6) Kitagawa, S.; Kitaura, R.; Noro, S. I. *Angew. Chem., Int. Ed.* **2004**, *43*, 2334–2375.
(7) Lee, J. Y.; Farha, O. K.; Roberts, J.; Scheidt, K. A.; Nguyen, S. B. T.; Hupp, J. T. *Chem. Soc. Rev.* **2009**, *38*, 1450–1459.
(8) Férey, G. *Chem. Soc. Rev.* **2008**, *37*, 191–214.
(9) Férey, G. *Dalton Trans.* **2009**, 4400–4415.
(10) Forster, P. M.; Cheetham, A. K. *Top. Catal.* **2003**, *24*, 79–86.
(11) Farrusseng, D.; Aguado, S.; Pinel, C. *Angew. Chem., Int. Ed.* **2009**, *48*, 7502–7513.
(12) Wang, Z.; Chen, G.; Ding, K. *Chem. Rev.* **2009**, *109*, 322–359.
(13) Long, J. R.; Yaghi, O. M. *Chem. Soc. Rev.* **2009**, *38*, 1213–1214.
(14) Maspoch, D.; Ruiz-Molina, D.; Veciana, J. *Chem. Soc. Rev.* **2007**, *36*, 770–818.
(15) Mueller, U.; Schubert, M.; Teich, F.; Puetter, H.; Schierle-Arndt, K.; Pastré, J. *J. Mater. Chem.* **2006**, *16*, 626–636.
(16) Morris, R. E.; Wheatley, P. S. *Angew. Chem., Int. Ed.* **2008**, *47*, 4966–4981.
(17) Horike, S.; Shimomura, S.; Kitagawa, S. *Nature Chem.* **2009**, *1*, 695–704.
(18) Janiak, C. *Dalton Trans.* **2003**, 2781–2804.
(19) Horcajada, P.; Chalati, T.; Serre, C.; Gillet, B.; Sebrie, C.; Baati, T.; Eubank, J. F.; Heurtaux, D.; Clayette, P.; Kreuz, C.; Chang, J. S.; Hwang, Y. K.; Marsaud, V.; Bories, P. N.; Cynober, L.; Gil, S.; Férey, G.; Couvreur, P.; Gref, R. *Nat. Mater.* **2010**, *9*, 172–178.
(20) Schlichte, K.; Kratzke, T.; Kaskel, S. *Microporous Mesoporous Mater.* **2004**, *73*, 81–88.

the framework, sometimes with interesting regioselectivity[27−29] or enantioselectivity.[32] Because of their very high surface area (often higher than 1000 m^2/g), the valorization of MOFs as support or templates for polyoxometalates, metal and metal oxide particles, is also investigated, opening new fields for catalytic applications.[33,36−40]

The design (eventually postfunctionalization) of a MOF *a priori*, according to the intended catalytic reaction, has been attempted several times in the examples cited before, mainly through the synthesis of structures exhibiting low-coordinated metal species as nodes (or at least labile ligands on the nodes),[41] or through the choice of appropriate linkers bearing an adequate chemical function. However, significant catalytic activities have also been reported for some "saturated" frameworks, e.g., without any low-coordinated structural metal atoms, and in which the linkers are not functionalized (if we except the linking function).[15,22,23,28,42,43] This "opportunistic" catalysis, as it was called by Hupp and co-workers,[7] is not well understood.

At this stage, provided no degradation of the MOF occurs under the operating conditions, three hypotheses can be drawn for the identification of the nature of the active site:

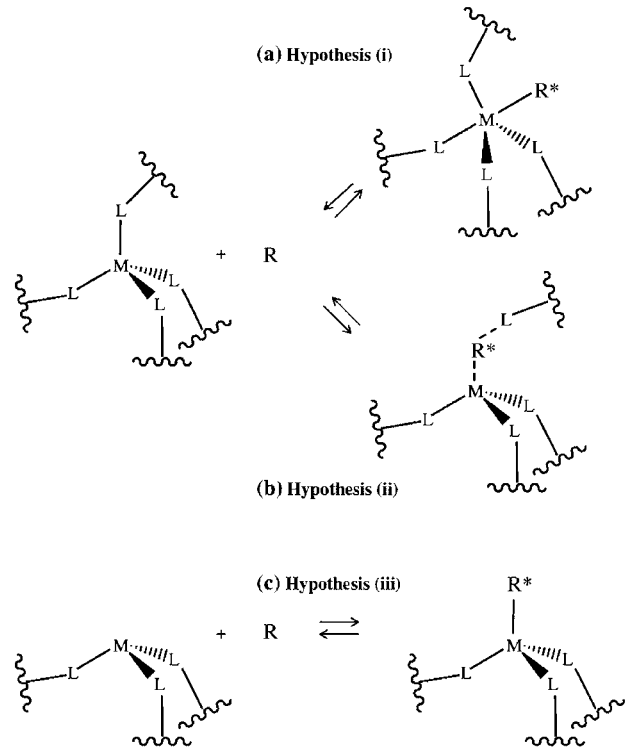

Figure 1. Hypotheses drawn for the explanation of the activation of a reactant R by a nonfunctionalized metal−organic framework (MOF). M depicts the node, L the linker of the MOF, and R* the activated reactant. (a) Hypothesis : Coordination promotion of the node (here from IV to V). (b) Hypothesis : Transient de-coordination of one M−L bond and subsequent activation of R by the low-coordinated M and/or L moieties. (c) Hypothesis : Activation at sites located on the external surface of the MOF or at structural defects, here exemplified by a M_{III} species.

(i)The apparently saturated node is temporarily able to increase even further its coordination number to achieve Lewis acid-type activation (Figure 1a).

(ii)One of the node-to-linker bonds temporarily de-coordinates to allow the generation of a transient species that is able to activate the reactants by either the Lewis acid moiety (unsaturated node) or the basic one (unsaturated linker), or both (Figure 1b). This has been proposed by Kwak et al.[42] to explain the activity of Zn-based coordination polymers in the transesterification of esters.

(iii)The external surface, or structural defects (as postulated by Ravon et al.[28] for the IRMOF-1 and -8 alkylation catalysts), of the MOF may be where the active sites are located, due to the expected presence of dangling bonds (Figure 1c).

Those proposals relate to the way organometallic complexes work in homogeneous catalysis, with additional constraints inherent to the (relative) rigidity of the framework. To date, no clear demonstration of the origin of catalysis on such materials has ever been provided. Molecular modeling can be of great help for rationalizing, at the atomic level, the behavior of MOFs and has often been used for that purpose. To the best of our knowledge, except for our very recent work focusing on the expected sites at the external surface of ZIF-8,[44] most atomistic approaches to the properties of MOFs are related to the defectless bulk of the material, mainly for storage and separation purposes (see refs 45−53 for examples). There is thus a great challenge in providing an atomistic picture of the reactive

(21) Alaerts, L.; Séguin, E.; Poelman, H.; Thibault-Starzyk, F.; Jacobs, P. A.; De Vos, D. E. *Chem.—Eur. J.* **2006**, *12*, 7353–7363.
(22) Horcajada, P.; Surblé, S.; Serre, C.; Hong, D. Y.; Seo, Y. K.; Chang, J. S.; Grenèche, J. M.; Margiolaki, I.; Férey, G. *Chem. Commun.* **2007**, 2820–2822.
(23) Llabrés i Xamena, F. X.; Abad, A.; Corma, A.; Garcia, G. *J. Catal.* **2007**, *250*, 294–298.
(24) Llabrés i Xamena, F. X.; Casanova, O.; Galiasso Tailleur, R.; Garcia, H.; Corma, A. *J. Catal.* **2008**, *255*, 220–227.
(25) Tanabe, K. K.; Cohen, S. M. *Angew. Chem., Int. Ed.* **2009**, *48*, 7424–7427.
(26) Ohara, K.; Kawano, M.; Inokuma, Y.; Fujita, M. *J. Am. Chem. Soc.* **2010**, *132*, 30–31.
(27) Thallapally, P. K.; Fernandez, C. A.; Motkuri, R. K.; Nune, S. K.; Liu, J.; Peden, C. H. F. *Dalton Trans.* **2010**, *39*, 1692–1694.
(28) Ravon, U.; Domine, M. E.; Gaudillère, C.; Desmartin-Chomel, A.; Farrusseng, D. *New J. Chem.* **2008**, *32*, 937–940.
(29) Liao, T. B.; Ling, Y.; Chen, Z. X.; Zhou, Y. M.; Weng, L. H. *Chem. Commun.* **2010**, *46*, 1100–1102.
(30) Platero Prats, A. E.; de la Pena-O'Shea, V. A.; Iglesias, M.; Snejko, N.; Monge, A.; Gutierrez-Puebla, E. *ChemCatChem* **2010**, *2*, 147–149.
(31) Ravon, U.; Savonnet, M.; Aguado, S.; Domine, M. E.; Janneau, E.; Farrusseng, D. *Microporous Mesoporous Mater.* **2010**, *129*, 319–329.
(32) Seo, J. S.; Whang, D.; Lee, H.; Jun, S. I.; Oh, J.; Jeon, Y. J.; Kim, K. *Nature* **2000**, *404*, 982–986.
(33) Hwang, Y. K.; Hong, D. Y.; Chang, J. S.; Jhung, S. H.; Seo, Y. K.; Kim, J.; Vimont, A.; Daturi, M.; Serre, C.; Férey, G. *Angew. Chem., Int. Ed.* **2008**, *47*, 4144–4148.
(34) Gascon, J.; Aktay, U.; Hernandez-Alonso, M. D.; van Klink, G. P. M.; Kapteijn, F. *J. Catal.* **2009**, *261*, 75–87.
(35) Savonnet, M.; Aguado, S.; Ravon, U.; Bazer-Bachi, D.; Lecocq, V.; Bats, N.; Pinel, C.; Farrusseng, D. *Green Chem.* **2009**, *11*, 1729–1732.
(36) Schröder, F.; Esken, D.; Cokoja, M.; van der Berg, M. W. E.; Lebedev, O. I.; Van Tendeloo, G.; Walaszek, B.; Buntkowsky, G.; Limbach, H. H.; Chaudret, B.; Fischer, R. A. *J. Am. Chem. Soc.* **2008**, *130*, 6119–6130.
(37) Opelt, S.; Türk, S.; Dietzsch, E.; Henschel, A.; Kaskel, S.; Klemm, E. *Catal. Comm.* **2008**, *9*, 1286–1290.
(38) Ishida, T.; Kawakita, N.; Akita, T.; Haruta, M. *Gold Bull.* **2009**, *42*, 267–274.
(39) Jiang, H. L.; Liu, B.; Akita, T.; Haruta, M.; Sakurai, H.; Xu, Q. *J. Am. Chem. Soc.* **2009**, *131*, 11302–11303.
(40) Juan-Alcaniz, J.; Ramos-Fernandez, E. V.; Lafont, U.; Gascon, J.; Kapteijn, F. *J. Catal.* **2010**, *269*, 229–241.
(41) Kitagawa, S.; Noro, S. I.; Nakamura, T. *Chem. Commun.* **2006**, 701–707.
(42) Kwak, H.; Lee, S. H.; Kim, S. H.; Lee, Y. M.; Park, B. K.; Lee, Y. L.; Jun, J. Y.; Kim, C. K.; Kim, S. J.; Kim, Y. *Polyhedron* **2009**, *28*, 553–561.
(43) Kwak, H.; Lee, S. H.; Kim, S. H.; Lee, Y. L.; Park, B. K.; Lee, E. Y.; Lee, Y. J.; Kim, C.; Kim, S. H.; Kim, Y. *Polyhedron* **2009**, *27*, 3484–3492.
(44) Chizallet, C.; Bats, N. *J. Phys. Chem. Lett.* **2010**, *1*, 349–353.

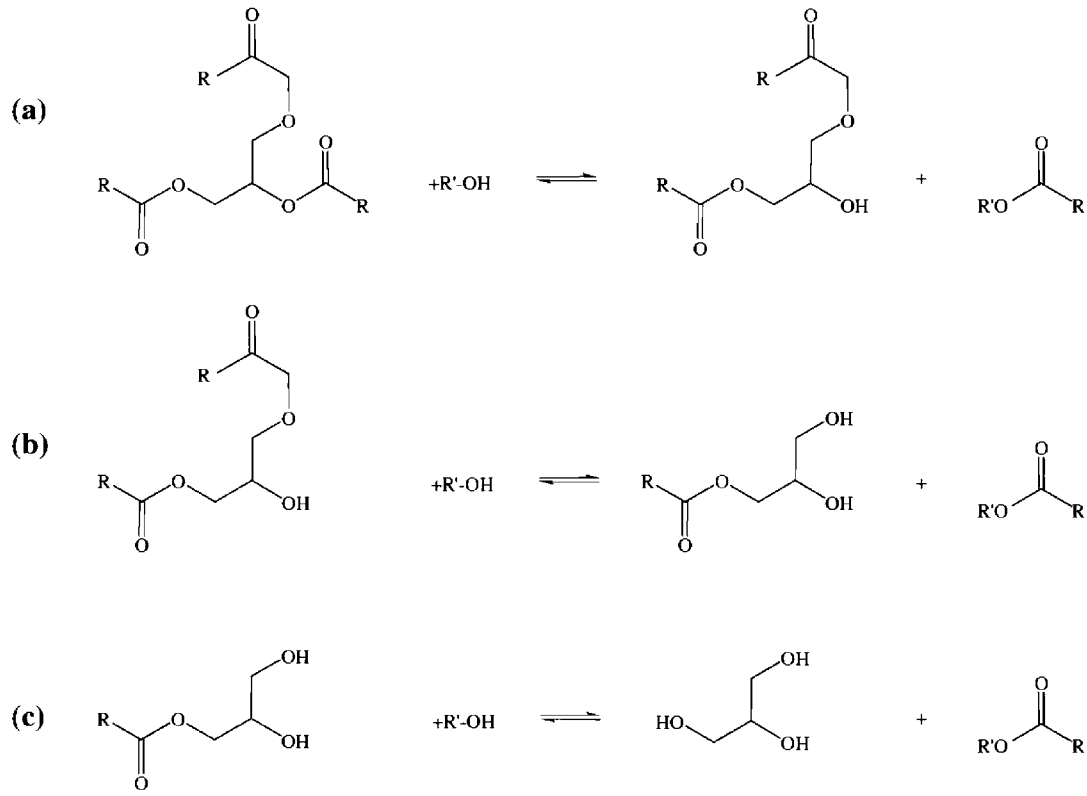

Figure 2. Successive steps in the transesterification of triglycerides with the R′OH alcohol, producing (a) diglycerides, (b) monoglycerides, and (c) glycerol, together with one molecule of ester RCOOR′ at each step.

behavior of these materials, according to the three hypotheses mentioned above.

One particularly interesting family of MOFs is the zeolite imidazolate frameworks (ZIFs).[54] ZIFs, based on an imidazolate linker and metallic nodes, can adopt symmetrical porous structures analogous to zeolites; for example, ZIF-8 has been synthesized from 2-methylimidazole (denoted Im in the following) and a zinc precursor in the sodalite form.[55,56] This zeolite-like material exhibits a high surface area of 1400 m^2/g, thermal stability up to 420 °C, and pore diameters of about 11 Å.[54,55] These properties make the ZIF-type materials good candidates for hydrogen and carbon dioxide storage applications.[57−62] *A priori*, catalysis should not be efficient on this type of material, insofar as Zn accommodates a very favorable tetrahedral coordination (as in the bulk of wurtzite ZnO, and in contrast to other very reactive Zn_V-based MOFs[42,63]) and no extra-functionalization on the 2-methylimidazolate linker.

In the present work, we show for the first time that despite this expected stability, ZIF-8 exhibits significant reactivity in transesterification of rapeseed oil (Figure 2) to produce alkyl esters. Methanol is traditionally one of the reactants, and then fatty acid methyl esters (FAME) are obtained and can be used as biodiesel.[64] We show here that ZIF-8 is a challenging alternative to zinc aluminate,[65] even allowing the use of alcohols other than methanol.

Such a reaction can be catalyzed by acids or bases. In particular, determining steps are the activation of the nucleophilicity of the alcohol by deprotonation (thanks to basic sites)

(45) Mulder, F. M.; Dingemans, T. J.; Wagemaker, M.; Kearley, G. *J. Chem. Phys.* **2005**, *317*, 113–118.
(46) Sun, Y. Y.; Kim, Y.-H.; Zhang, S. B. *J. Am. Chem. Soc.* **2007**, *129*, 12606–12607.
(47) Sillar, K.; Hofmann, A.; Sauer, J. *J. Am. Chem. Soc.* **2009**, *131*, 4143–4150.
(48) Salles, F.; Ghoufi, A.; Maurin, G.; Bell, R. G.; Mellot-Draznieks, C.; Férey, G. *Angew. Chem., Int. Ed.* **2008**, *47*, 8487–8491.
(49) Boutin, A.; Springuel-Huet, M. A.; Nossov, A.; Gédéon, A.; Loiseau, T.; Volkringer, C.; Férey, G.; Coudert, F. X.; Fuchs, A. H. *Angew. Chem., Int. Ed.* **2009**, *48*, 8314–8317.
(50) Han, S. S.; Goddard, W. A., III *J. Am. Chem. Soc.* **2007**, *129*, 8422–8423.
(51) Han, S. S.; Mendoza-Cortés, J. L.; Goddard, W. A., III *Chem. Soc. Rev.* **2009**, *38*, 1460–1476.
(52) Perez-Pellitero, J.; Amrouche, H.; Siperstein, F.; Pirngruber, G.; Nieto-Draghi, C.; Chaplais, G.; Simon-Masseron, A.; Bazer-Bachi, D.; Peralta, D.; Bats, N. *Chem.—Eur. J.* **2010**, *16*, 1560–1571.
(53) Liu, D.; Zhong, C. *J. Phys. Chem. Lett.* **2010**, *1*, 97–101.
(54) Phan, A.; Doonan, C. J.; Uribe-Romo, F. J.; Knobler, C. B.; O'Keeffe, M.; Yaghi, O. M. *Acc. Chem. Res.* **2010**, *43*, 58–67.
(55) Huang, X. C.; Lin, Y. Y.; Zhang, J. P.; Chen, X. M. *Angew. Chem., Int. Ed.* **2006**, *45*, 1557–1559.
(56) Parks, K. S.; Ni, Z.; Coté, B.; Choi, J. Y.; Huang, R. D.; Uribe-Romo, F. J.; Chae, H. K.; O'Keeffe, M.; Yaghi, O. M. *Proc. Natl. Acad. Sci. U.S.A.* **2006**, *103*, 10186–10191.
(57) Hayashi, H.; Côté, A. P.; Furukawa, H.; O'Keeffe, M.; Yaghi, O. M. *Nat. Mater.* **2007**, *6*, 501–506.
(58) Banerjee, R.; Phan, A.; Wang, B.; Knobler, C.; Furukawa, H.; O'Keeffe, M.; Yaghi, O. M. *Science* **2008**, *319*, 939–943.
(59) Wang, B.; Côté, A. P.; Furukawa, H.; O'Keeffe, M.; Yaghi, O. M. *Nature* **2008**, *453*, 207–212.
(60) Wu, H.; Zhou, W.; Yildirim, T. *J. Am. Chem. Soc.* **2007**, *129*, 5314–5315.
(61) Banerjee, R.; Furukawa, H.; Britt, D.; Knobler, C.; O'Keeffe, M.; Yaghi, O. M. *J. Am. Chem. Soc.* **2009**, *131*, 3875–3877.
(62) Moggach, S. A.; Bennett, T. D.; Cheetham, A. K. *Angew. Chem., Int. Ed.* **2009**, *48*, 7087–7089.
(63) Nuzhdin, A. L.; Dybtsev, D. N.; Fedin, V. P.; Bukhtiyarova, G. A. *Dalton Trans.* **2009**, 10481–10485.
(64) Ballerini, D. *Les Biocarburants: Etat des lieux, perspectives et enjeux de développement*; Editions Technip: Paris, 2006.
(65) Pugnet, V.; Maury, S.; Coupard, V.; Dandeu, A.; Quoineaud, A. A.; Bonneau, J. L.; Tichit, D. *Appl. Catal., A* **2010**, *374*, 71–78.

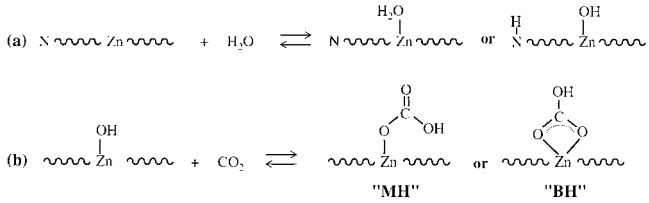

Figure 3. Expected behavior of water and carbon dioxide on the external surface of ZIF-8. (a) Molecular or dissociative adsorption of water. (b) Formation of monodentate (MH) and bidentate (BH) hydrogenocarbonates.

and the activation of the electrophilicity of the ester (thanks to Brønsted or Lewis acid sites). Following hypothesis (Figure 1a), acid activation can be invoked on Zn_{IV} nodes. Hypothesis raises the additional questions of the acidity of Zn_{III} ions and the basicity of the methylimidazolate moiety within the framework. The same kind of sites (Zn_{III} and N^- extremities of the linkers) can be exposed on the surface. Depending on the number of linkers lost around an exposed Zn center, Zn_{II} and Zn_I could also be found, of course with different stabilities. After synthesis, the samples are usually exposed to air, which can lead to adsorption of water and/or CO_2 on these reactive sites. In particular, water can adsorb molecularly (on exposed Zn) or dissociatively (on $Zn^{2+}-N^-$ pairs, Figure 3a), generating OH and NH groups. CO_2 can further lead to the formation of hydrogenocarbonates (Figure 3b), either monodentate (noted in the following as "MH") or bidentate ("BH"). We have proposed an *ab initio* evaluation of the stability of these various sites.[44] Their acido-basicity now has to be looked at in detail to understand the reactivity of ZIF-8.

In the present work, we combine FTIR-monitored carbon monoxide adsorption at low temperature and density functional theory (DFT) calculations to investigate the nature of acido-basic sites in the porosity and on the surface of ZIF-8. Carbon monoxide is indeed very commonly used to get a first insight on potentially reactive Lewis and Brønsted acid sites,[66−68] including for MOFs.[21,69,70] We show here that information can also be obtained on potentially basic sites. Periodic and cluster models of the solid are associated to obtain the most accurate picture of the behavior of Zn nodes (in the bulk or at the external surface) with reactants and to assign experimental infrared spectra. The adsorption ability of CO is then compared with that of methanol and of a model ester, methyl acetate, so as to identify the active site in the reaction.

To the best of our knowledge, this study is the first to demonstrate the catalytic interest of ZIF-8 and provides a thorough demonstration of the location of the active sites by both analytical and *ab initio* calculations techniques. The concepts established here may be of great interest for understanding the behavior of the external surface of the whole ZIF family; more generally, they can provide a rationale for catalysis by nonfunctionalized MOFs.

(66) Lavalley, J. C. *Catal. Today* **1996**, *27*, 377–401.
(67) Lercher, J. A.; Gründling, C.; Eder-Mirth, G. *Catal. Today* **1996**, *27*, 353–376.
(68) Knözinger, H. In *Handbook of Heterogeneous Catalysis*; Ertl, G. Knözinger, H.; Weitkamp, J., Eds.; Wiley: Weinheim, 1997; Vol. 2, pp 707−732.
(69) Bordiga, S.; Regli, L.; Bonino, F.; Groppo, E.; Lamberti, C.; Xiao, B.; Wheatley, P. S.; Morris, R. E.; Zecchina, A. *Phys. Chem. Chem. Phys.* **2007**, *9*, 2676–2685.
(70) Chavan, S.; Bonino, F.; Vitillo, J. G.; Groppo, E.; Lamberti, C.; Dietzel, P. D. C.; Zecchina, A.; Bordiga, S. *Phys. Chem. Chem. Phys.* **2009**, *11*, 9811–9822.

2. Experimental Part

2.1. Synthesis. The synthesis of ZIF-8 was carried out with slight modifications to the procedure reported by Huang et al.[55] A solution consisting of 2-methylimidazole (6.442 g, Sigma-Aldrich, 99%) dissolved in 100 mL of methanol (SDS, HPLC grade 99.8%) was slowly added to a solution of zinc hydroxide (3.904 g, International Laboratory, 95%) in aqueous ammonia (25% v/v, 500 mL, Carlo-Erba). White polyhedral crystals began to appear immediately. Synthesis was done under ambient temperature with gentle steering. After 2 days, the resulting white solid was filtered off and washed three times with 100 mL of a H_2O/MeOH (1:1v/v) mixture. This solid was dried in air and characterized by elemental analysis, X-ray diffraction (XRD), and N_2 adsorption isotherms.

Zinc aluminate was used as a reference material for the catalytic activity. This catalyst was prepared using a method previously described.[65] A commercial boehmite was mixed with ZnO powder in the presence of a nitric acid solution. This mixture was kneaded for about 45 min and then extruded in order to form cylinders. Theses extrudates were then dried overnight at 593 K and calcined at 1173 K. The catalyst obtained is a zinc aluminate with a Zn/Al ratio of 0.3.

2.2. Characterizations. The textural properties of the ZIF-8 sample were analyzed by recording the N_2 adsorption isotherm at 77 K, using a Micromeritics ASAP 2420 instrument. Before gas sorption analysis, ZIF-8 was pretreated for 12 h at 383 K under vacuum. The specific surface area was determined using the Brunauer−Emmett−Teller (BET) model.

Powder XRD patterns were collected on a Bruker D4 X-ray diffractometer with Cu Kα radiation at 40 kV, 40 mA and fitted with an energy-discriminating detector. 2θ angles were scanned from 2° to 60° at a rate of 0.02°/s. Elemental analyses were performed by X-ray fluorescence (for Zn) and thermal conductivity measurements (for N, O, C, and H).

Infrared spectra were recorded on a Nexus Fourier transform instrument equipped with a KBr beam splitter and an MTC nitrogen-cooled detector. Infrared spectra of self-supporting pellets of pure powder sample, inserted in a liquid nitrogen-cooled IR cell (CaF_2 windows) connected to a conventional gas-manipulation evacuation line, were collected with 4 cm^{-1} resolution. The ZIF-8 sample was pretreated from 298 to 473 K within 4 h under vacuum ($\sim 10^{-6}$ mbar). The sample was then outgassed during 10 h at 473 K under vacuum ($\sim 10^{-6}$ mbar). CO adsorption was performed *in situ* at low temperature (liquid N_2 temperature) by applying pulses of increasing CO pressures and constant volume (1.69 mL) (corresponding to CO amounts from 0.3 to 292 μmol).

2.3. Catalytic Tests. Experiments were performed in a 100 mL stainless steel batch reactor. The reaction medium was stirred with a magnetic stirring bar and heated with a heating magnetic stirrer. Reactants (commercial alcohols and edible-grade rapeseed oil) and catalyst (0.5 g) were first introduced in the reactor. The molar alcohol/oil ratio was set at 27.5, as the nature of the alcohol could change for the study. The total mass of liquid was set at 50 g. The reaction medium was then stirred at 200 rpm and heated at 473 K. The time $t = 0$ was assigned when the temperature reached 473 K, which explains nonzero conversion at $t = 0$.

The initial reaction medium and the reaction effluents form a biphasic mixture at ambient temperature (however, it is monophasic at 473 K), the polar phase containing mainly glycerol and unreacted alcohol, and the apolar phase containing

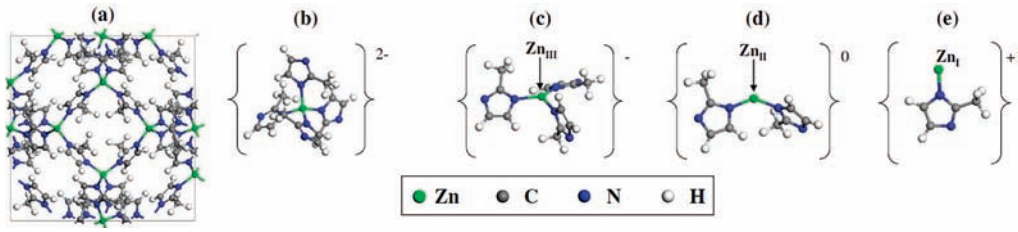

Figure 4. Systems modeled by DFT: (a) bulk ZIF-8 (periodic approach); (b) {Zn-Im$_4$} cluster; (c) {Zn-Im$_3$} cluster; (d) {Zn-Im$_2$} cluster; and (e) {Zn-Im$_1$} cluster.

mainly FAME (or other esters when alcohols other than methanol are used) and glycerides. Sample of 2 mL were collected manually from the reaction medium, at different reaction times, for analysis. The samples were washed with brine in order to remove glycerine and the alcohol. Eight drops of the apolar phase (containing glycerides and FAME) were then diluted in 3 mL of analytical-grade THF, and the sample was analyzed by gel permeation chromatography on a Waters HPLC apparatus equipped with three Waters Styragel columns (THF) with a molar mass range of 0−1000 g·mol^{-1}. These columns were placed in a thermostated oven at 313 K. Detection was made using a Waters 2414 refractive index detector. The results gave the relative composition of the apolar phase in triglycerides, diglycerides, monoglycerides, and FAME. At the end of the reaction, the reaction medium was collected and filtered on a 0.1 μm Teflon filter, and extra alcohol was evaporated. The apolar phase (containing ester and nonconverted glycerides) and the polar phase (containing glycerine and ethers) were separated and analyzed by ICP-OES, to analyze eventual catalyst leaching products. The apparatus used was a Thermo Jarrell Ash Iris Advantage inductively coupled plasma optical emission spectrometer. The apolar-phase samples were diluted in xylene and directly injected, whereas the polar-phase samples were diluted in ethanol and injected via a cold (−10 °C) nebulization chamber.

Zinc aluminate was chosen as a reference catalyst, as the use of this kind of solid has been described in a heterogeneous industrial transesterification process.

3. Computational Methods

3.1. Periodic Approach. Periodic density functional calculations were performed with the VASP 4.6 code,[71] in the framework of the generalized gradient approximation (GGA) of Perdew and Wang (PW91).[72] The interaction between core and valence electrons was described by the projector augmented waves (PAW) approach[73] with an energy cutoff of 400 eV. Due to the dimensions (cubic unit cell of 17.012 Å per side) of the cell considered, all calculations were performed at the gamma point. Geometry optimizations were run until residual forces on atoms did not exceed 5×10^{-2} eV·Å^{-1}. Gaussian smearing with $\sigma = 0.05$ eV was applied. Figure 4a depicts the bulk of ZIF-8 after optimization of the atomic positions at constant lattice parameter (extracted from Huang et al.[55]). The cell contains 276 atoms. As explained in our previous work,[44] periodic systems also enabled the cluster approach described in the next paragraph to be validated.

3.2. Cluster Approach. A cluster approach was chosen to model the local environment of reactive sites of ZIF-8 at a higher level of theory than GGA, in particular for the accurate calculation of the vibration frequencies of the adsorbed CO molecule. Cluster density functional calculations were performed in the framework of the hybrid B3LYP exchange-correlation functional,[74,75] with the def2-TZVPP basis set, within the TURBOMOLE 5.10 code[76,77] via the MAPS 3.1 platform (distributed by Scienomics). In a preliminary work,[44] we extensively studied the impact of the size of the cluster and of the basis set, which led to the parameters chosen here. Four main types of environments of Zn have been modeled (Figure 4b−e): {Zn-Im$_i$}$^{(2-i)+}$ (Im being the ligand) are representative of the local environment of the Zn ions within the structure of the MOF ($i = 4$) or at its external surface ($i = 1-3$, depending on the number of metal−ligand links lost). For the sake of clarity, these clusters will be denoted {Zn-Im$_i$} ($i = 1-4$) in what follows, without any further mention on their charge. The geometry of {Zn-Im$_4$} was fully optimized (until residual forces on atoms did not exceed 5×10^{-2} eV·Å^{-1}), but the Zn atom only was allowed to relax in {Zn-Im$_{1-3}$}, to take into account the rigidity of the real periodic ZIF-8 structure. The validity of the present cluster approach was established by comparison with periodic systems (see ref 44). The interaction of these sites with H_2O and CO_2 was studied[44] to quantify the thermal stability of adsorbed molecular water and CO_2 molecules, hydroxyls, NH groups, and hydrogenocarbonates (MH and BH, Figure 3). First, the adsorption energies of water and/or CO_2 were compared to establish the stability at 0 K of the various systems. The impact of the temperature and of the pressure was then taken into account by calculating free energies, $\Delta_r G$, according to the model presented in ref 44.

The adsorption of CO on the relevant acido-basic sites was further modeled (the adsorbing site and CO molecule being relaxed). Harmonic vibration frequencies were determined analytically in TURBOMOLE. Anharmonic corrections were applied for one case (CO adsorption on the Zn atom of {Zn-Im$_3$}): the potential energy surface was explored manually, by varying the C≡O distance in the range ±0.05 Å, the mass center of the vibrator being fixed. A grid of 11 points was used to fit the potential energy variations with a third-order development of the Morse potential, and the anharmonic stretching frequency was deduced from the resolution of the Schrödinger equation for the Morse potential and from the fit parameters. By this method, it was shown that the CO frequency shift, $\Delta\nu_{CO} = \nu_{CO(adsorbed)} - \nu_{CO(g)}$, between the adsorbed state and the gas phase is the same with or without anharmonicity corrections. Thus, only CO harmonic frequency shifts are reported in what follows. The adsorption of methanol and methyl acetate was then investigated on the most plausible sites in the operating conditions (as obtained from the thermodynamic approach).

4. Experimental Results

The XRD pattern (Supporting Information, Figure S1.1) was indexed in a cubic symmetry with $a = 17.050(8)$ Å (close to sample 1 reported by Huang et al.[55]). The elemental analysis provides the following results (weight percent): Zn, 27.59; O,

(71) Kresse, G.; Hafner, J. *Phys. Rev. B* **1994**, *49*, 14251–14269.
(72) Perdew, J.; Wang, Y. *Phys. Rev. B* **1992**, *45*, 13244–13249.
(73) Kresse, G.; Joubert, D. *Phys. Rev. B* **1999**, *59*, 1758–1775.
(74) Becke, A. D. *J. Chem. Phys.* **1993**, *98*, 5648–5652.
(75) Lee, C.; Yang, W.; Parr, R. G. *Phys. Rev. B* **1988**, *37*, 785–789.
(76) Ahlrichs, R.; Bär, M.; Häser, M.; Horn, H.; Kölmel, C. M. *Chem. Phys. Lett.* **1989**, *162*, 165–169.
(77) Treutler, O.; Ahlrichs, R. *J. Chem. Phys.* **1995**, *102*, 346–354.

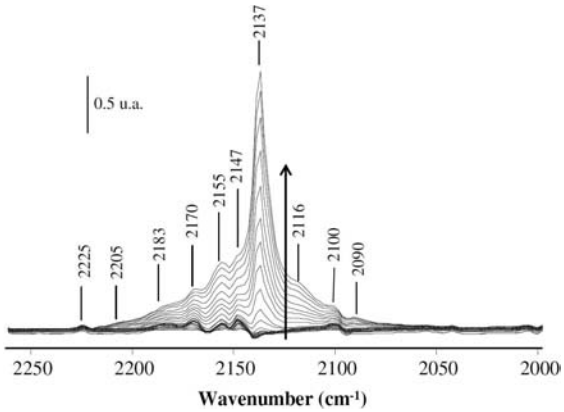

Figure 5. FTIR difference spectra of ZIF-8 recorded after adsorption of CO, in the C≡O zone. The arrow indicates increasing amounts of CO.

3.50; N, 23.23; H, 4.23; C, 41.15. The calculated values for $(ZnC_8N_4H_{10})_{12}(CO_2)_{2.1}(H_2O)_{2.1}$ are as follow: Zn, 27.43; O, 3.52; N, 23.49; H, 4.38; C, 41.18. This confirms that ZIF-8 was properly synthesized. Type I nitrogen sorption isotherm (Supporting Information, Figure S2.1) behavior was observed for ZIF-8, confirming its microporous nature. It also revealed a permanent open porosity. An apparent surface area of 1460 $m^2 \cdot g^{-1}$ was obtained using the BET model, in line with the literature.

4.1. Characterization of Acido-Basicity by CO Adsorption Monitored by FTIR. The FTIR spectrum of the material after activation at 473 K under vacuum (Supporting Information, Section S3) is compatible with spectra reported in the literature for this material.[62] In addition to framework bands, peaks at frequency higher than 3200 cm^{-1} were observed, despite very low intensities relative to the others. Spectra recorded for increasing amounts of adsorbed CO (from 0.3 to 292 μmol, with the spectrum of the activated sample subtracted) are reported in Figure 5 for the C≡O vibration frequency domain. In the 3900−3200 cm^{-1} region, a set of new bands grows upon CO adsorption (not shown). Due to the very small intensities recorded in this domain, no comment on the evolution of the corresponding band can be made because of the low signal/noise ratio. This is, however, an indication that the species vibrating in this zone are affected by CO adsorption. We focus on the C≡O region in the following.

For the smallest CO doses, a 2225 cm^{-1} band appeared first, strongly blue-shifted (+82 cm^{-1}) as compared to that for gas-phase CO (~2143 cm^{-1}). Other blue-shifted bands (2205−2147 cm^{-1}) then gradually appear, accompanied by some strongly red-shifted components at 2100 (−43 cm^{-1}) and 2090 cm^{-1} (−53 cm^{-1}). These negative shifts are of the same order of magnitude as those reported for O-adducts (see further section 5.2) on alkaline-exchanged zeolites.[78,79] Finally, for higher CO coverage, a band near 2147 cm^{-1} grows, with a side peak near 2116 cm^{-1}. Note that the position of the peaks observed at very low CO coverage was almost unaffected by the increase in the amount of adsorbed CO. This suggests that, in contrast to ZnO for example,[80,81] only poor dipolar coupling occurs between CO molecules, and adsorbing sites are well defined and isolated.

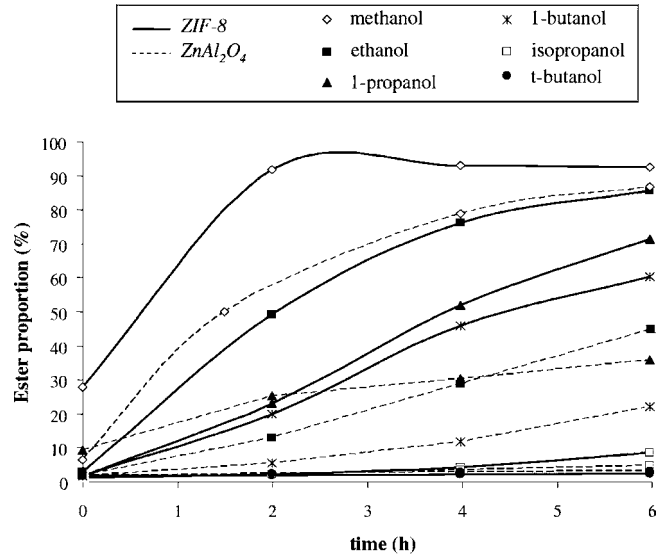

Figure 6. Conversion of vegetable oil into monoglyceride at 473 K, catalyzed by ZIF-8, as a function of time, depending on the nature of the alcohol (reference data on a conventional $ZnAl_2O_4$ catalyst are also given).

4.2. Transesterification of Vegetable Oil. The reaction of vegetable oil with methanol at 473 K, in the presence of ZIF-8 as a catalyst, led to the full conversion into monoglycerides in less than 2 h. This corresponds to a significant improvement in catalytic properties as compared to a conventional $ZnAl_2O_4$ catalyst, as shown in Figure 6. Leaching of zinc was estimated at about 100 ppm in the glycerol and 1 ppm in the ester, which is an indication of the heterogeneous origin of the activity recorded here. Moreover, the reactivity is dependent on the nature of the alcohol involved in the reaction. Linear alcohols (methanol, $pK_A = 15$; ethanol, $pK_A = 16$; 1-propanol and 1-butanol, $pK_A \approx 19$) as well as branched ones (isopropanol, $pK_A = 17$; *tert*-butanol, $pK_A = 19$) were tested (Figure 6). The reactivity decreases with the acidity of linear alcohols; however, branched alcohols exhibit almost no reactivity. The same trend were observed for ZIF-8 and $ZnAl_2O_4$, showing that the limited reactivity of branched alcohols was not due to diffusion problems in the porosity of ZIF-8. For each alcohol, the reactivity of ZIF-8 was improved as compared to the reference $ZnAl_2O_4$ catalyst.

5. DFT Results

5.1. External Surface Sites of ZIF-8 as a Function of Temperature and Pressure. The diagram depicted in Figure 7 summarizes the stability of the various groups located at the external surface of ZIF-8,[44] depending on the number of Im linkers still bonded to the Zn node. $P = 1$ bar represents the conditions in ambient air; $P = 10^{-3}$ mbar is typical of analytical conditions (FTIR cell). The partial pressures of CO_2 and water are given by the composition of ambient air. Experimentally, the pressure measured on the gauge was lower (~10^{-6} mbar), but the pressure at the level of the wafer is certainly higher, so a better evaluation of the stability of the species is given by calculations done at $P = 10^{-3}$ mbar.

At 0 K, hydrogenocarbonates (monodentate, MH) are always the most stable species (Figure 7a,d,i). Then, by increasing the

(78) Arean, C. O.; Tsyganenko, A. A.; Platero, E. E.; Garrone, E.; Zecchina, A. *Angew. Chem., Int. Ed.* **1998**, *37*, 3161–3163.
(79) Garrone, E.; Fubini, B.; Bonelli, B.; Onida, B.; Otero Arean, C. *Phys. Chem. Chem. Phys.* **1999**, *1*, 513–518.
(80) Scarano, D.; Bertanione, S.; Spoto, G.; Zecchina, A.; Otero Arean, C. *Thin Solid Films* **2001**, *400*, 50–55.
(81) Scarano, D.; Spoto, G.; Bordiga, S.; Zecchina, A.; Lamberti, C. *Surf. Sci.* **1992**, *276*, 281–298.

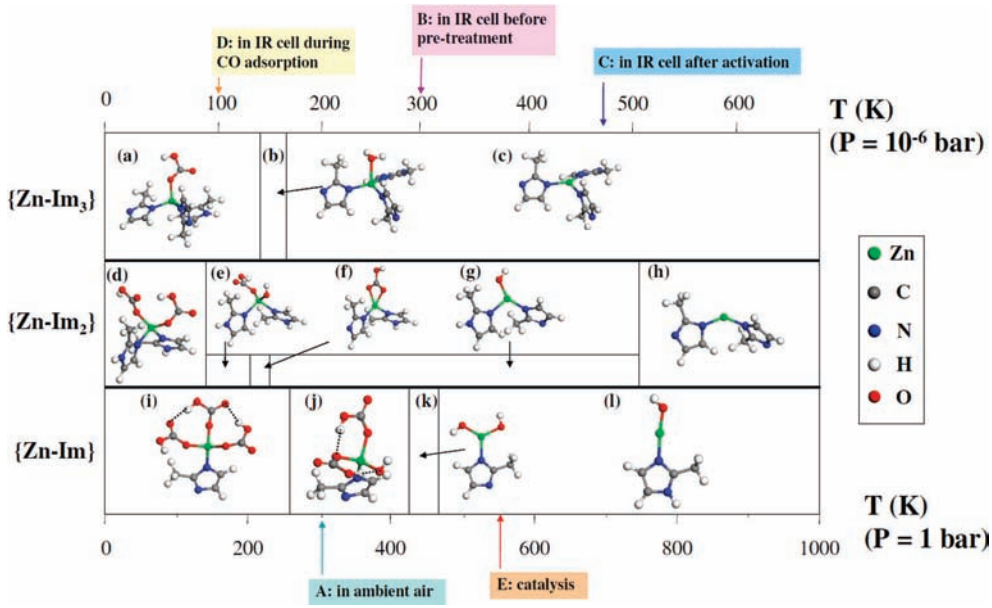

Figure 7. Structure and thermal stability of adsorbates on {Zn-Im$_i$} clusters, for a total pressure of 1 bar (lower axis) and 10^{-6} bar (upper axis) in air. (a) MH and NH on {Zn-Im$_3$}, (b) molecular water on {Zn-Im$_3$}, and (c) {Zn-Im$_3$} without any adsorbate. (d) Two MH and two NH on {Zn-Im$_2$}, (e) one MH, one OH, and two NH on {Zn-Im$_2$}, (f) one BH and NH on {Zn-Im$_2$}, (g) one OH and NH on {Zn-Im$_2$}, and (h) {Zn-Im$_2$} without any adsorbate. (i) Three MH on {Zn-Im}, (j) two MH and one OH on {Zn-Im}, (k) two OH on {Zn-Im}, and (l) one OH and one NH on {Zn-Im}. A−E refer to experimental operating conditions during pretreatment, analysis, and catalysis (see text).

temperature, MH gradually convert into OH groups by the release of CO_2, or eventually into bidentate hydrogenocarbonates (Figure 7f). On Zn_{III} ({Zn-Im$_3$} cluster), molecular water is more favorable than dissociated water (Figure 7b). Zn_{III} is then revealed from water desorption on {Zn-Im$_3$} at ∼230 K in ambient air (Figure 7c). Zn_{III} species, surrounded by one or two OH groups (on {Zn-Im$_2$} and {Zn-Im$_1$}, respectively, Figure 7g,k), also appear at ∼210 and 410 K, respectively (in ambient air). Zn_{II} are expected at higher temperatures from {Zn-Im$_2$} and {Zn-Im$_1$} (Figure 7h,l), but Zn_I species (issued from the ultimate dehydration of {Zn-Im$_1$}) never appear on the stability diagram due to their significant reactivity toward water.

From Figure 7, it is possible to infer the species present during the experimental procedure before CO adsorption. At ambient temperature and pressure (mark A in Figure 7), Zn_{III} species are thus found on {Zn-Im$_3$} and {Zn-Im$_2$}, together with OH and NH groups on {Zn-Im$_2$} and {Zn-Im}, and MH groups on {Zn-Im}. Under lower pressure (sample put into vacuum, mark B in Figure 7) at ∼298 K, the calculations predict the desorption of CO_2 and H_2O from {Zn-Im}, leading to the formation of Zn_{III} and geminal OH groups. Upon thermal treatment at ∼473 K (mark C in Figure 7), Zn_{II} and isolated Zn_{II}−OH groups should be obtained on {Zn-Im}. Lowering the temperature to about 100 K (just before CO introduction, mark D in Figure 7) produces MH groups on all kind of {Zn-Im$_i$} systems, converting all Zn_{III} into Zn_{IV}. The calculated stability ranges at low temperature are however quite narrow, and this, together with the impact of the kinetics of re-adsorption of H_2O and CO_2, can lead to a great variety of environments, which must be taken into account in assigning the experimental spectra reported in section 4.1.

At this stage, the best evaluation of the surface species in the catalytic test is given by the conditions at 1 bar and 473 K, even if the presence of the alcohol as the main species in the medium is not taken into account in the calculations. In these conditions, we mainly expect Zn_{III} and Zn_{II} on the surface (Figure 7, mark E), eventually with OH groups (on {Zn-Im$_2$} and {Zn-Im}). NH are also expected, in same amount as OH groups.

5.2. Interaction of Bulk and Surface Sites with CO. 5.2.1. Various Modes Studied. The adsorption of CO was then modeled, first to propose an assignment for the experimental spectra (section 4.1) and more generally to identify the sites that are able to exhibit some specific functionality. The three hypotheses given in the Introduction [extension of the coordination of the Zn_{IV} node; de-coordination of imidazolate ligands from Zn nodes, revealing Zn^{2+} and N^- reactive moieties; and reactivity of the sites located at the external surface of ZIF-8] were computationally explored. Additionally, the interaction of the CO molecule with the Im ligands was calculated. Figure 8 summarizes the CO adsorption modes studied, with some examples.

The main adsorption energies of the CO molecule and shifts of the stretching C≡O frequencies, calculated on the basis of the cluster models, are reported in Table 1. Usually, the CO molecule interacts through its C atom with transition metals. In the present case we deal with a cationic Zn^{2+} species, so that the electrostatic component of the interaction may prevail.[82,83] Shifts can thus be assigned in part to the vibrational Stark effect. However, Scarano et al. showed for ZnO that a small orbital overlap of σ type cannot be excluded.[81] Orbitals calculations were performed to address that point.

For small interaction strengths, a mutual equilibrium was found between C- and O-adducts.[78,79,84−90] Thus, we investi-

(82) Pacchioni, G.; Cogliandro, G.; Bagus, P. S. *Surf. Sci.* **1991**, *255*, 344–354.
(83) Storozhev, P. Y.; Yanko, V. S.; Tsyganenko, A. A.; Turnes Palomino, G.; Rodriguez Delgado, M.; Otero Arean, C. *Appl. Surf. Sci.* **2004**, *238*, 390–394.
(84) Ferrari, A. M.; Neyman, K. M.; Rösch, N. *J. Phys. Chem. B.* **1997**, *101*, 9292–9298.
(85) Tsyganenko, A. A.; Escalona Platero, E.; Otero Arean, C.; Garrone, E.; Zecchina, A. *Catal. Lett.* **1999**, *61*, 187–192.

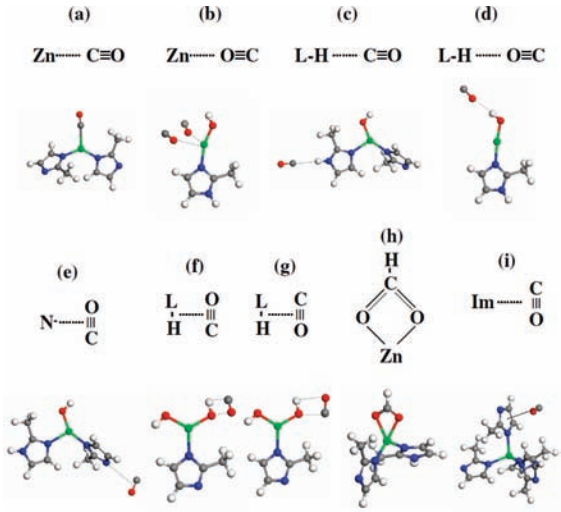

Figure 8. Adsorption modes of CO invoked in the present computational study and examples of optimized cluster structures: (a) C-adduct with Zn^{2+}; (b) O-adducts with of Zn^{2+}; (c) C-adduct with L−H groups (L = O, N, M, B); (d) O-adduct with L−H groups (L = O, N, M, B); (e) side-on mode with N^-; (f) side-on mode with L−H, L−H||OC; (g) side-on mode with L−H, L−H||CO; (h) formate; and (i) interaction of CO with the Im cycle. Same colors as in Figure 7.

gated both types of linear adsorption modes with potentially Lewis (Figure 8a,b) and Brønsted (Figure 8c,d) acid/basic sites. With anionic species like oxygen in zeolites frameworks, a side-on mode was shown as the most stable.[91] This mode was studied for N^- terminations (Figure 8e). We will also show that this kind of mode can be obtained in a more general manner (CO adsorbed parallel to the LH groups, L = O, N, M, or B, Figure 8f,g). Formates (Figure 8h) were also reported to result from reaction of CO on nucleophilic OH groups (on MgO and γ-Al_2O_3,[92] zirconia,[93,94] partially reduced ceria,[95] and ZnO[96]), so we also quantified their stability *ab initio*. Finally, adsorption configurations of CO in the vicinity of the imidazolate ligand were calculated (Figure 8i), by analogy with the observations on benzene rings in mesoporous organosilicas.[88]

5.2.2. Interaction of CO with the Bulk of ZIF-8. Within the ZIF-8 framework, the coordination of CO by Zn_{IV} nodes is expected to lead to Zn_V (Figure 1a). Any attempt to simulate the Zn coordination extension in the bulk of ZIF-8 on the basis of periodic or cluster models (Figure 4a,b) failed, CO being ejected from the coordination sphere of Zn. The breaking of one Zn−N bond within the framework to stabilize the CO molecule in the neighborhood of a newly formed Zn_{III} atom (Figure 1b), and eventually by the N^- moiety of the de-coordinated Im, was modeled by the periodic approach but corresponds to a highly endothermic reaction (+120 kJ·mol^{-1} for the C-adduct; ejection of the CO molecule and re-formation of the Zn−N bond for the O-adduct). Finally, the most stable mode of interaction of CO with the ZIF-8 framework appeared to be interaction with the Im ligands themselves, as depicted in Figure 8i and in Supporting Information Figure S4.1 (−8 kJ·mol^{-1} with the periodic model and −7 kJ·mol^{-1} with the {Zn-Im_4} cluster model). As for benzene in organosilicas,[88] the CO molecule preferentially adsorbs parallel to the aromatic ring. The frequency shift is, however, very low, +2 cm^{-1}, near the gas-phase frequency. This can explain the growing 2137 cm^{-1} mode, dominant for the highest CO adsorbed amounts (Figure 5).

5.2.3. Interaction of CO with External Lewis Sites. For the sites representative of the external surface of ZIF-8, we considered not only the most stable systems in the operating conditions (low pressure, $T \approx 100$ K) but also all other systems which appear in the thermodynamic diagram (Figure 7), as some of them are likely to be obtained after pretreatment at 473 K.

Calculations (Table 1) predict that the most stable species are C-adducts (from one to three CO molecules on the same site) involving Zn_I and Zn_{II} Lewis acid sites (Figure 8a). They also give rise to the highest C≡O frequency blue-shift (up to +95 cm^{-1}), as expected. Because such low coordination numbers are not stabilized easily in the medium (see the thermodynamic diagram), they are presumably in the minority as compared to surface Zn_{III} and Zn_{IV}. The highest adsorption energy values are consistent with the appearance of the 2225 and 2205 cm^{-1} bands from the first pulses of CO in the experimental IR spectrum. As reported in section 5.2.2, Zn_{IV} is unable to interact with CO molecules. Zn_{III} species interact much more weakly with CO molecules than Zn_{II} (no stronger adsorption than −8 kJ·mol^{-1}) and accordingly lead to lower blue-shifts (+16 cm^{-1} or lower), consistent with the 2155 cm^{-1} experimental band. Note that, for ZnO samples, CO adsorption experiments led to shifts of about +50 cm^{-1} at low coverage.[80,97] For the {Zn-Im_2} cluster on which two CO molecules are adsorbed, no back-donation was shown, but bonding overlap takes place between d orbitals of Zn and the HOMO of CO (σ-donor) (Supporting Information, Figure S5.1). Thus, as inferred by Scarano et al. for ZnO,[81] blue-shifts induced by Lewis Zn^{2+} sites are due to both electrostatic and orbital overlap (σ-type) effects.

O-adducts on Zn^{2+} Lewis sites were also calculated (Figure 8b) and led either to slightly positive frequency shifts for the weakest sites (+4 cm^{-1} for the Zn_{III}···OC adduct in {Zn-Im_3}, but the adsorption energy is only −1 kJ/mol) or to strongly negative shifts on Zn_{II} (−49 cm^{-1} for Zn_{II}···OC), which can explain the 2100 and 2090 cm^{-1} experimental bands. O-adducts were always less stable than C-adducts on Lewis acid sites probed here. To our knowledge, this is the first time that this mode is shown for and O-adduct involving Zn^{2+} as Lewis sites, most studies reported in the literature being focused mainly on alkali metal cation-exchanged zeolites.

(86) Otero Arean, C.; Tsyganenko, A. A.; Manoilova, O. V.; Turnes Palomino, G.; Penarroya Mentruit, M.; Garrone, E. *Chem. Commun.* **2001**, 455–456.
(87) Storozhev, P. Y.; Otero Arean, C.; Garrone, E.; Ugliengo, P.; Ermoshin, V. A.; Tsyganenko, A. A. *Chem. Phys. Lett.* **2003**, *374*, 439–445.
(88) Camarota, B.; Ugliengo, P.; Garrone, E.; Arean, C. O.; Delgado, M. R.; Inagaki, S.; Onida, B. *J. Phys. Chem. C* **2008**, *112*, 19560–19567.
(89) Bonelli, B.; Otero Arean, C.; Armandi, M.; Rodriguez Delgado, M.; Garrone, E. *ChemPhysChem* **2008**, *9*, 1747–1751.
(90) Bucko, T.; Hafner, J.; Benco, L. *J. Phys. Chem. B* **2005**, *109*, 7345–7357.
(91) Tsyganenko, A. A.; Kondratieva, E. V.; Yanko, V. S.; Storozhev, P. Y. *J. Mater. Chem.* **2006**, *16*, 2358–2363.
(92) Gopal, P. G.; Schneider, R. L.; Watters, K. L. *J. Catal.* **1987**, *105*, 366–372.
(93) Pokrovski, K.; Taek Jung, K.; Bell, A. T. *Langmuir* **2001**, *17*, 4297–4303.
(94) Korhonen, S. T.; Calatayud, M.; Krause, A. O. *J. Phys. Chem. C* **2008**, *112*, 16096–16102.
(95) Li, C.; Sakata, Y.; Domen, K.; Maruya, K. I.; Onishi, T. *J. Chem. Soc., Faraday Trans. 1* **1989**, *85*, 1451–1461.
(96) Hussain, G.; Sheppard, N. *Spectrochim. Acta, Part A* **1987**, *43*, 1631–1637.
(97) Griffin, G. L.; Yates, J. T. *J. Chem. Phys.* **1982**, *77*, 3751–3758.

Table 1. Calculated CO Frequency Shift (in Decreasing Order) and Adsorption Energy Related to Stable Adsorption Modes of CO on Various Sites of ZIF-8, Modeled by the Cluster Approach[a]

calculated $\Delta\nu_{CO}$ (cm^{-1})	cluster	adsorbates on the Zn nucleus	adsorption mode	adsorption energy per CO molecule ($kJ \cdot mol^{-1}$)
+89, +95, +100	{Zn-Im}	no adsorbate	Zn_I ···· 3 CO	−79
+86, +92	{Zn-Im}	no adsorbate	Zn_I ···· 2 CO	−94
+83	{Zn-Im}	OH(1) + NH(1)	Zn_{II}···· 1 CO	−32
+68, +77	{Zn-Im}	OH(1) + NH(1)	Zn_{II} ···· 2 CO	−30
+65	{Zn-Im}	no adsorbate	Zn_I ···· 1 CO	−117
+63	{Zn-Im_2}	no adsorbate	Zn_{II} ···· 1 CO	−37
+51, +59	{Zn-Im_2}	no adsorbate	Zn_{II} ···· 2 CO	−29
+51	{Zn-Im}	OH(1) + NH(1)	Zn_{II}−Im−NH ···· CO	−20
+35	{Zn-Im}	OH(1) + NH(1)	Zn_{II}−OH ···· CO	−13
+29	{Zn-Im_2}	OH(1) + NH(1)	Zn_{III} −Im−NH ···· CO	−10
+16	{Zn-Im_3}	no adsorbate	Zn_{III} ···· CO	−8
+16	**{Zn-Im_3}**	MH(1) + NH(1)	**Zn_{IV}−Im−NH ···· CO**	−6
+13	{Zn-Im_2}	OH(1) + NH(1)	Zn_{III} ···· CO	−4
+9	**{Zn-Im_3}**	**MH(1) + NH(1)**	**Zn_{IV}−MH ···· CO**	**−5**
+9	{**Zn-Im_2**}	MH(2) + NH(2)	**Zn_{IV}−MH ···· CO**	**−4**
+9	{Zn-Im_2}	BH(1) + NH(1)	Zn_{IV}−BH ···· CO	−10
+8	{Zn-Im_2}	OH(1) + NH(1)	Zn_{III}−OH ···· CO	−3
+7	**{Zn-Im}**	**MH(3)**	**Zn_{IV}−MH ···· CO**	**−13**
+6	**{Zn-Im}**	**MH(3)**	**Zn_{IV}−MH ···· OC**	**−4**
+6	**{Zn-Im_2}**	**MH(1) + OH(1) + NH(2)**	**Zn_{IV}−MH ···· CO**	**−3**
+4	{Zn-Im_3}	no adsorbate	Zn_{III} ···· OC	−1
+4	**{Zn-Im_2}**	**MH(1) + OH(1) + NH(2)**	**Zn_{IV}−OH ···· OC**	**−1**
+2	**periodic (bulk)**		**Im‖CO**	**−8**
0	**{Zn-Im_2}**	**MH(1) + OH(1) + NH(2)**	**Zn_{IV}−OH ···· CO**	**−2**
0	{Zn-Im_3}	molecular H_2O (1)	Zn_{IV}−OH ···· CO	−10
−2	{Zn-Im_2}	OH(1) + NH(1)	Zn_{III}−OH ···· OC	−1
−3	{Zn-Im_2}	OH(1) + NH(1)	Zn_{III}−OH‖CO	−2
−3	**{Zn-Im}**	**MH(3)**	**Zn_{IV}−MH‖CO**	**−5**
−5	{Zn-Im_2}	OH(1) + NH(1)	Im−N^-‖CO	−3
−6	**{Zn-Im}**	**MH(3)**	**Zn_{IV}−MH‖OC**	**−6**
−6	{Zn-Im_3}	molecular H_2O (1)	Zn_{IV}−OH ···· OC	−6
−16	{Zn-Im_2}	OH(1) + NH(1)	Zn_{III}−Im−NH ···· OC	−5
−22	{Zn-Im}	OH(1) + NH(1)	Zn_{II}−OH ···· OC	−6
−33	{Zn-Im}	OH(2)	Zn_{III} −OH‖OC	−13
−38	{Zn-Im}	OH(1) + NH(1)	Zn_{II}−Im−NH ···· OC	−11
−43	{Zn-Im}	OH(2)	Zn_{III} −OH‖CO	−12
−43, −47	{Zn-Im}	OH(1) + NH(1)	Zn_{II} ···· 2 OC	−8
−49	{Zn-Im}	OH(1) + NH(1)	Zn_{II} ···· 1 OC	−9

[a] The simulated local structures are also given. "‖" indicates side-on modes. The most likely species in the operating conditions according to the thermodynamic diagram (Figure 7, mark D) are emphasized in bold.

5.2.4. Interaction of CO with External NH Groups. NH groups appeared to be the strongest Brønsted acid sites, on the basis of both the CO adsorption energies within the C-adduct mode (Figure 8c, up to −20 $kJ \cdot mol^{-1}$) and the corresponding C≡O frequency shifts (up to +51 cm^{-1}). These features were enhanced when the Im ligand was bonded to Zn_{II} (as compared to Zn_{III} and Zn_{IV}). They can be considered as partially responsible for the 2205, 2170, and 2155 cm^{-1} bands for Zn_{II}-Im-NH, Zn_{III}-Im-NH, and Zn_{IV}-Im-NH, respectively. O-adducts are also stable (even if less stable than C-adducts, as in the case of protonic sites in zeolites[86,88] or silicas[87,88]) on N−H groups and lead to negative frequency shifts (up to −11 cm^{-1} for Zn_{II}-Im-NH), generally lower than those of zeolites. These modes likely participate in the 2137 and 2100 cm^{-1} experimental bands. Finally, side-on adducts were tested on NH groups but were never stable.

5.2.5. Interaction of CO with External OH Groups. Except for the Zn_{II}-OH groups, which were the site of competitive interaction of CO (C-adduct) as compared to NH groups (+35 cm^{-1} frequency shift with −13 $kJ \cdot mol^{-1}$ stabilization), other C-adduct on OH groups induced only weak interaction and low frequency shifts (+8 cm^{-1} and lower). This is an indication of poor Brønsted acidity. The O-adducts on OH groups (again generally less stable than C-adducts, Figure 8d) generally led to negative frequency shifts, likely at the origin of the 2137 and 2116 cm^{-1} experimental bands. The most favorable CO adducts on OH groups were side-on modes (up to −13 $kJ \cdot mol^{-1}$; see for example Figure 8f,g)., which are expected to take part in the 2137, 2116, and 2100 cm^{-1} experimental bands. With typical formation energies of −80 to −133 $kJ \cdot mol^{-1}$, formates appeared to be by far more stable than all CO adducts (Figure 8h). However, no clear experimental infrared evidence can be given here for formates, probably due to kinetic limitations: their formation requires much more demanding bond-breaking and -forming sequences[98] than the simple formation of adducts, as evidenced by the elevated temperatures (higher than 100 K) required for their formation on oxides.[92,93,96]

5.2.6. Interaction of CO with External Hydrogenocarbonates. Due to their stability range (low temperature), hydrogenocarbonates (MH and BH) are exclusively bonded to Zn_{IV} species. They are thus only weak Brønsted acid sites, as shown by their moderate adsorption energies relative to the C-adducts. The 2155 cm^{-1} band can be assigned to those species. O-adducts and side-on modes were competitive with C-adducts on hydrogenocarbonates. Most of them led to slightly negative shifts, which can be linked to the 2137 cm^{-1} band.

(98) Calatayud, M.; Collins, S. E.; Baltanas, M. A.; Bonivardi, A. L. *Phys. Chem. Chem. Phys.* **2009**, *11*, 1397–1405.

Table 2. Calculated Adsorption Energies of Methanol and Methyl Acetate on External Surface Sites of ZIF-8, Related to Stable Species in the Catalytic Test Conditions (Mark E in Figure 7)

		adsorption energy ($kJ \cdot mol^{-1}$)	
cluster	adsorbates	of methanol	of methyl acetate
{Zn-Im_3}	no adsorbate	−31 (molec.)	−16
{Zn-Im_2}	OH(1) + NH(1)	−35 (dissoc. on Zn and OH)	−30 (on Zn_{III})
		−46 (molec.)	−36 (on NH)
{Zn-Im}	OH(1)	−58 (molec.)	−40
		−76 (dissoc. on Zn and N^-)	

5.2.7. Interaction of CO with External N^- Moieties. Among the various types of CO adducts with the N^- moieties studied, only the side-on adduct (Figure 8e) appeared to be stable, with a small red-shift of the CO stretching frequency (-5 cm^{-1}), similar to that observed for silica, whereas oxide ions in the CsX zeolite induced a stronger red shift (~ -20 cm^{-1}).[91]

The most stable surface species in the considered operating conditions are indicated by mark D in Figure 7. The corresponding expected signals are emphasized in bold in Table 1. They appear in a narrow range ([−6,+16 cm^{-1}]) around the $\Delta\nu_{CO} = 0$ cm^{-1} value, which means that, statistically, the signal is expected to be mostly developed in the spectral region around 2143 cm^{-1}, which is indeed the case (see Figure 5).

5.3. Interaction of Bulk and Surface Sites with Alcohols.

5.3.1. Interaction of Methanol with the Bulk of ZIF-8. The activation of methanol on the Zn_{IV} nodes within the bulk (periodic model) was explored according to hypotheses and (Figure 1): both extension of coordination of Zn_{IV} to Zn_V and activation by de-coordination of a Zn−N bond failed with methanol (extension of the coordination led to ejection of methanol within the pore, with an interaction energy of −15 $kJ \cdot mol^{-1}$, and de-coordination of the Zn−N bond corresponds to a very endothermic process, +113 $kJ \cdot mol^{-1}$), as for CO. It can thus be definitely concluded that activation of the reactants will not occur easily on the nodes located in the bulk of ZIF-8.

5.3.2. Interaction of Methanol with Surface Sites of ZIF-8. The adsorption of methanol on the external surface of ZIF-8 was modeled on the clusters identified as the most stable in the given operating conditions (catalytic test, mark E in Figure 7). Molecular and dissociative adsorption (dissociation of the O−H bond, adsorption of CH_3O^- on Zn_{III} and Zn_{II}, and protonation of N^- moieties or OH groups) were investigated. Adsorption energies are reported in Table 2 for the preferred adsorption modes. Adsorption on external surface sites was preferred over adsorption within the bulk. Similarly to water adsorption, methanol adsorbed molecularly on the Zn_{III} atom of {Zn-Im_3}. On {Zn-Im_2}, molecular and dissociative adsorption of methanol are very competitive (−46 and −35 $kJ \cdot mol^{-1}$ for the molecular and dissociative modes, respectively). Dissociation preferentially occurred by protonation of the OH group, and a strong hydrogen bond remained between the CH_3O^- groups and the water molecule that was obtained (Figure 9a). On {Zn-Im}, dissociation was more favorable than molecular adsorption and preferentially involved Zn_{II} cations and N^- anions. Comparison of the adsorption energies from one system to another indicates that the adsorption is more favorable on Zn_{II} than on Zn_{III}, as expected. However, it is more favorable on Zn_{III} of {Zn-Im_2} than on {Zn-Im_3}, which can tentatively be assigned to two factors:

(1)Steric hindrance: indeed the OH group on {Zn-Im_2} is less bulky than the additional Im linker in {Zn-Im_3}.

(2)Electronic factors: OH groups may render the Zn−O slightly more ionic than the Zn−N bond between the node and the linker.

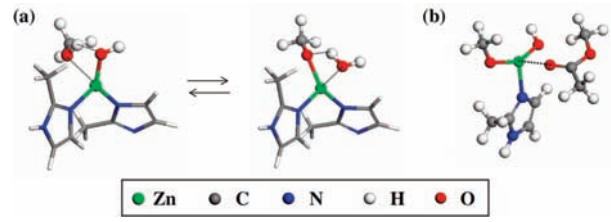

Figure 9. (a) Competitive adsorption modes of methanol on Zn_{III} (as modeled on the {Zn-Im_2} cluster with one OH group on Zn), either molecular (left) or dissociation on Zn-OH pairs (right). (b) Co-adsorption of methyl acetate and methanol (dissociation on Zn-N pairs) on Zn_{II} of the {Zn-Im} clusters.

This could enhance the effective Lewis acidity of Zn_{III} in {Zn-Im_2} as compared to {Zn-Im_3}. However, CO adsorption energies and frequency shifts (Table 1) are almost the same for both systems.

5.4. Interaction of Surface Sites with Methyl Acetate. Triglycerides are too bulky (see an evaluation of their dimensions by force-field simulations in the Supporting Information, Section S6) to enter the bulk of ZIF-8. This, together with the fact that alcohols themselves cannot be activated in the bulk of the catalyst (section 5.3), led us to consider the activation of esters at the external surface of ZIF-8 only.

Methyl acetate was chosen as a model ester for DFT calculations. Its adsorption on the external surface of ZIF-8 was modeled by the same method as for the adsorption of methanol. Activation by the Zn_{III} and Zn_{II} atoms was investigated, as well as protonation by NH groups. Adsorption energies are reported in Table 2. As for methanol, adsorption of methyl acetate is more favorable on Zn_{II} than on Zn_{III}, even if the sensitivity of methyl acetate is less pronounced than that of methanol. The activation on NH groups is competitive with that on Zn_{III} (on {Zn-Im_2}) and Zn_{II} (on {Zn-Im}), but the ester is not protonated in its most stable state (NH interacts with the ester through hydrogen-bonding).

The transesterification reaction then requires a certain proximity between the activated alcohol and ester partners. Among the Zn surface sites accessible in catalytic conditions, only Zn_{II} species have the opportunity to adsorb (and thus activate) at the same place the two molecules. The explicit co-adsorption was calculated for the {Zn-Im} cluster exhibiting one OH group. The resulting structure is shown in Figure 9b. The global co-adsorption energy reached −91 $kJ \cdot mol^{-1}$. As shown by Zn−O bond lengths (2.39 Å for the ester and 1.86 Å for the methanolate species) and by adsorption modes, the methanol molecule is more strongly activated than the ester, consistent with the strong dependence of the catalytic activity on the alcohol acidity (section 4.2).

6. Discussion

The present work shows for the first time that ZIF-8 can be a very interesting catalyst in the transesterification reaction, despite the absence of postfunctionalization, and the reaction proceeds with several linear alcohols (methanol, ethanol, 1-propanol, and 1-butanol). The infrared spectrum of the material suggests that some OH- and NH-type species exist on the sample. DFT cluster calculations indeed indicate that a great variety of species can be expected on the external surface of ZIF-8: Zn_{III} and Zn_{II} ions, N^- moieties of nonbridging linkers, OH and NH groups, as well as hydrogenocarbonates (monodentates MH or bidentates BH).

Table 3. Assignments of FTIR Spectra for CO Adsorption on the External Surface of ZIF-8, As Obtained from DFT Calculations

Experimental $\Delta\nu_{CO}$ (cm^{-1})	Assignment from calculations				
	Lewis sites		Brønsted sites		
	C adduct	O adduct	C adduct	O adduct	Side-on adducts
+82	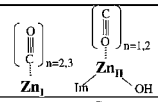	-	-	-	-
+62	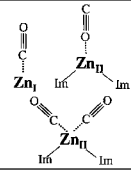	-	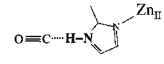	-	-
+40	-	-	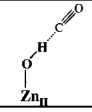	-	-
+27	-	-	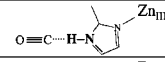	-	-
+12		-	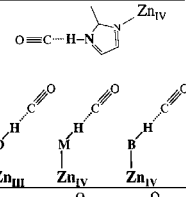	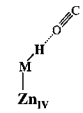	-
+4	-		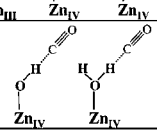	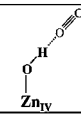	-
-6	-	-	-	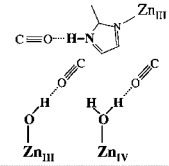	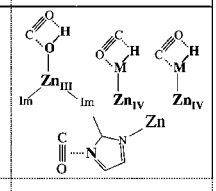
-27	-	-	-	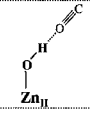	
-43	-		-	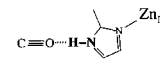	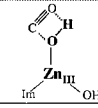
-53	-		-	-	-

The CO molecule, the adsorption of which was followed by FTIR, was used to get a closer look at the nature of the acido-basic sites. On the basis of periodic and cluster DFT calculations, we propose first an assignment of the experimental infrared spectra and then an identification of the acido-basic sites in the bulk and on the surface of the solid. We then discuss the plausible active sites in catalysis on the basis of results obtained by simulation of the adsorption of methanol and methyl acetate on ZIF-8.

6.1. Assignment of Infrared Spectra (C≡O Stretching Frequencies). CO adsorption on ZIF-8 activated at 473 K in a vacuum leads to a variety of bands in the infrared, in the C≡O stretching frequency region of the spectrum. Several bands correspond to blue-shifts as compared to CO in the gas phase, which is an indication of the presence of C-adducts of CO with acid sites of the solid up to strong sites (as attested by the shift to $+82$ cm^{-1}). More surprisingly (because of their lower occurrence in the literature), a set of red-shifted bands appears from the first CO pulses. Indeed, the bands observed are barely shifted as a function of CO coverage. The first question arising from these results has to do with where CO adsorbs at low coverage: Does the external surface play a role, or does CO only reveal peculiar interactions with the bulk material itself?

DFT calculations indicate that CO interacts only weakly with the bulk of ZIF-8 and cannot be responsible for strong infrared shifts. In contrast, species at the external surface of the material are shown to induce various interactions, some of them being quite strong. Various adsorption modes (C-adducts, O-adducts, side-on adducts) are indicated and explain the spectral features observed experimentally. The assignment of the IR spectra, as suggested by calculations, is reported in Table 3. C-adducts are

mostly responsible for the blue-shift region of the spectra, whereas O-adducts and side-on adducts are at the origin of the red-shifted zone.

Except on Zn_{II} and Zn_{I}, where several CO molecules can adsorb, the sites interacting with CO are well separated (generally by a distance equivalent to the dimensions of the linker, which plays the role of the constitutive anion), in contrast to inorganic materials, where bonding sites are very close to one another (for example, on ZnO, oxide ions are the only species separating the Zn^{2+} cations). This specificity allows the convenient determination of the acido-basicity of the sites probed.

6.2. Multifunctionality at the Organic−Inorganic Interface As Viewed by CO. Such an approach reveals strong Lewis acid sites on the surface of ZIF-8. Indeed, for ZnO samples, CO adsorption experiments led to shifts of at most $+50$ cm^{-1}.[80,97] As the Zn_{III} modeled in the present work induces only a weak shift of $+12$ cm^{-1}, we can assign the presence of stronger Lewis acid sites to the higher occurrence of Zn_{II} on ZIF-8 than of ZnO (Zn_{I} is too reactive to exist in significant amounts). NH groups are the strongest Brønsted acid sites on the solid. According to the strong blue-shift generated ($+51$ cm^{-1} from calculations), they could be stronger Brønsted acid sites than H−Y zeolites, for example.[86] Other protonic groups (OH and hydrogenocarbonates) do not exhibit significant Brønsted acidity. They induce mainly side-on adducts with CO, which is an indication of possible basicity. N^- moieties of nonbridging linkers are also potentially basic sites, as shown by CO adsorption. Thus, the external surface of ZIF-8 exhibits a set of species which develop specific acido-basicity. This suggests that catalysis occurs on the external surface, supporting hypothesis given in the Introduction. At this stage, CO adsorption does not validate hypotheses and , as no de-coordination seems possible (periodic calculations).

6.3. Catalysis by Nonfunctionalized ZIF-8. We show that ZIF-8 catalyzes very efficiently the transesterification of vegetable oil by methanol. The reaction rate decreases with the acidity of the linear alcohol (from methanol to ethanol, 1-propanol, and 1-butanol), which suggests that the activation of the alcohol proceeds via its deprotonation. The bulkiness of the triglycerides (too high to allow diffusion into ZIF-8), together with the absence of activation of methanol (the most reactive alcohol) in the bulk of ZIF-8, as shown by DFT calculations, leads us to exclude any reactivity from the bulk and to assign catalysis mainly to the external surface of the material. Bulky alcohols (isopropanol and *tert*-butanol) are hardly converted in the presence of ZIF-8, which could be interpreted as being due to the porosity of the material. But the same is observed in the presence of the $ZnAl_2O_4$ reference catalyst: an intrinsic limitation is thus shown for the reaction of ramified alcohols.

Among the hypotheses depicted in Figure 1, hypothesis is thus validated. The thermodynamic diagram of stable species at the surface obtained from the theoretical approach enables the species present in catalytic conditions to be identified. In particular, Zn_{III} and Zn_{II} species are exposed, together with OH groups, NH groups, and free N^- moieties. Esters can be activated on Zn_{III}, Zn_{II}, and NH groups (even if protonation does not correspond to an energy minimum in the latter case). Acid (Zn_{III} or Zn_{II})−base (OH or N^-) pairs are shown to be able to deprotonate methanol, but the most interesting species, capable of activating both the ester and the alcohol in very close regions, is Zn_{II}, likely surrounded by one linker and one OH group. This is consistent with CO-FTIR experiments, which show that the strong Lewis acidity is mainly due to Zn_{II}. We thus propose that these sites are responsible for catalysis.

For the reaction of interest in the present work, we can exclude catalysis within the pores due to strong steric hindrance in the glycerides. However, for smaller reactants, one could also invoke confinement effects to explain such catalytic properties. We also cannot exclude that, for some other reactions, defects within the solid would reveal some low-coordinated Zn cations and N^- moieties, for which our cluster simulation may also apply and which may exhibit catalytic activity. The purposeful introduction of point defects in the structure of ZIF-8, as was done for MOF-5 very recently,[31] could make it possible to further enhance the catalytic properties of this kind of material.

7. Conclusion

The high catalytic activity of one of the most popular zeolite imidazolate frameworks, ZIF-8, is illustrated in the transesterification of vegetable oil with various alcohols (methanol, ethanol, 1-propanol, 1-butanol, isopropanol, and *tert*-butanol). The reactivity increases with the acidity of the linear alcohol. However, ZIF-8, composed of saturated tetrahedral Zn nodes and methylimidazolate linkers coordinated to Zn nodes by each of their reactive parts, is not a functionalized MOF, so the origin of its catalytic properties can be questioned. We performed carbon monoxide adsorption at low temperature and monitored it by FTIR to evaluate the acido-basicity of the solid. A combination of cluster and periodic DFT calculations enabled the infrared spectra to be assigned and a structural model for the active sites to be proposed.

Three hypotheses were explored for the origin of such catalytic activity: Are Zn nodes able to increase their coordination to activate the reactants? Do Zn−N bonds dissociate to achieve activation by Zn_{III} and N^- moieties? Are the active sites unsaturated cations or specific groups located at the external surface of the material? Hypotheses and were theoretically addressed on the basis of a periodic model of the material. To investigate the third hypothesis, we built an *ab initio* cluster model, taking into account the various coordination modes possible for Zn, as well as the presence of water and carbon dioxide in the atmosphere. The stability of the various species was evaluated on the basis of a thermodynamic model coupled to DFT results. Depending on temperature and pressure, hydroxyls, NH groups, hydrogenocarbonates, low-coordinated Zn atoms, and free N^- moieties belonging to linkers are shown to coexist on the external surface of ZIF-8.

The FTIR spectra obtained after CO adsorption at low temperature on ZIF-8 activated at 473 K under a vacuum are very complex in the C≡O stretching frequency region. Not only are traditional blue-shifts at various frequencies observed, up to $+82$ cm^{-1} as compared to the gas phase, but also a set of red-shifted signals. Using DFT cluster calculations, these signals were assigned to classical C-adducts of CO with acid sites (blue-shifts), as well as O-adducts and side-on adducts on acid and basic sites. Moreover, we demonstrate that the sites that have a significant impact on the vibrational properties of CO are located at the external surface of the material, and not in the porosity of ZIF-8. This approach shows that some strong Lewis sites exist (in particular Zn_{II} species), as well as strong Brønsted acid sites (NH groups), together with basic sites (OH groups and N^- moieties mainly).

Taking into account these findings, and explicitly simulating the co-adsorption of a model ester (methyl acetate) and methanol, we show that ZIF-8 is able to dissociate alcohols, in line with experimental catalytic results demonstrating a prevailing role of the acidity of this reactant. Zn_{II} species as acid sites, located at the external surface (or possibly in bulk defects of ZIF-8), combined with N^- moieties and OH groups as basic ones, are shown to be particularly interesting for the combined activation of alcohols and esters and are proposed as the active sites. This work opens new perspectives on the use of nonfunctionnalized MOFs in catalysis, and more generally on the understanding of the external surface properties (such as hydrophilicity/hydrophobicity) of all kinds of MOFs.

Acknowledgment. All calculations have been performed at IFP HPC center and at IDRIS/CINES HPC centers within the project x2010086335 funded by GENCI.

Supporting Information Available: Figures S1−S6, showing XRD patterns, nitrogen sorption isotherms, and FTIR spectra of ZIF-8, interactions of CO with ZIF-8, $CO\cdots Zn^{2+}$ bonding in $\{Zn\text{-}Im_2\}$, and comparison of the dimensions of tri-, di-, and monoglycerides to ZIF-8. This material is available free of charge via the Internet at http://pubs.acs.org.

JA103365S